HHS Public Access

Author manuscript

J Thromb Haemost. Author manuscript; available in PMC 2024 December 30.

Published in final edited form as:

J Thromb Haemost. 2019 December ; 17(12): 2022–2034. doi:10.1111/jth.14597.

Platelet-type von Willebrand disease: Local disorder of the platelet GPIbα β-switch drives high-affinity binding to von Willebrand factor

Alexander Tischer,
Venkata R. Machha,
Laurie Moon-Tasson,
Matthew Auton

Division of Hematology, Departments of Internal Medicine and Biochemistry and Molecular Biology, Mayo Clinic, Rochester, MN, USA

Abstract

Background: Mutations in the β-switch of GPIbα cause gain-of-function in the platelet-type von Willebrand disease. Structures of free and A1-bound GPIbα suggest that the β-switch undergoes a conformational change from a coil to a β-hairpin.

Objectives: Platelet-type von Willebrand disease (VWD) mutations have been proposed to stabilize the β-switch by shifting the equilibrium in favor of the β-hairpin, a hypothesis predicated on the assumption that the complex crystal structure between A1 and GPIbα is the high-affinity state.

Methods: Hydrogen-deuterium exchange mass spectrometry is employed to test this hypothesis using G233V, M239V, G233V/M239V, W230L, and D235Y disease variants of GPIbα. If true, the expectation is a decrease in hydrogen-deuterium exchange within the β-switch as a result of newly formed hydrogen bonds between the β-strands of the β-hairpin.

Results: Hydrogen—exchange is enhanced, indicating that the β-switch favors the disordered loop conformation. Hydrogen—exchange is corroborated by differential scanning calorimetry, which confirms that these mutations destabilize GPIbα by allowing the β-switch to dissociate from the leucine-rich-repeat (LRR) domain. The stability of GPIbα and its A1 binding affinity, determined by surface plasmon resonance, are correlated to the extent of hydrogen exchange in the β-switch.

Correspondence Matthew Auton, Division of Hematology, Departments of Internal Medicine and Biochemistry and Molecular Biology, Mayo Clinic, Rochester, MN 55905, USA. auton.matthew@mayo.edu.

AUTHOR CONTRIBUTIONS

VRM and LMT produced and purified the proteins. VRM performed SPR experiments. AT performed and analyzed DSC, SEC, Fluorescence, CD, and HXMS experiments. AT and MA wrote the manuscript. MA designed the study.

SUPPORTING INFORMATION

Additional supporting information may be found online in the Supporting Information section at the end of the article.

CONFLICTS OF INTEREST

The authors state that they have no conflict of interest.

Conclusion: These studies demonstrate that GPIbα with a disordered loop is binding-competent and support a mechanism in which local disorder in the β-switch exposes the LRR—domain of GPIbα enabling high-affinity interactions with the A1 domain.

Keywords

GPIbα; von Willebrand factor; β-switch

1 | INTRODUCTION

A rheologically malleable bond between the von Willebrand factor (VWF) and platelets is essential to primary hemostasis and necessary for subsequent coagulation and the arrest of bleeding. This bond between the VWF A1 domain and the platelet VWF receptor, GPIbα, occurs under the rheological shear of blood flow, which unravels large multimeric species of VWF exposing the A1 domains to platelet GPIbα.[1] It must be strong enough to recruit platelets to sites of vascular injury, weak enough so as to not be prothrombotic, but not too weak as to obviate the interaction altogether. The autosomal dominant inherited von Willebrand disease (VWD) and the platelet-type von Willebrand disease (PT-VWD), constitute two sides of this macromolecular coin in which genetic mutations cause amino acid substitutions in the A1 domain and in GPIbα, respectively, thereby altering the intrinsic binding affinity of this interaction. (a) A1 domain mutations cause both gain-of-function and loss-of-function phenotypes resulting in the more common Type 2B and Type 2M qualitative subtypes of VWD. (b) Mutations in GPIbα cause a gain-of-function, which is often difficult to identify and distinguish from Type 2B VWD[2,3] without gene sequencing of both VWF and GPIbα.[4] Compared to Type 2B VWD, PT-VWD is rare, with less than 60 patients identified worldwide.[5,6] Like extreme cases of Type 2B VWD, PT-VWD can manifest in loss of high molecular weight multimers of VWF and thrombocytopenia in patients especially in situations that stimulate elevated VWF levels such as pregnancy, stress, and infection.[2]

A structural basis for high—affinity between A1 and GPIbα in general to both Type 2B VWD and PT-VWD has remained elusive. Over the last two decades, fifteen structures have been determined of the WT (wild-type),[7] Type 2B,[8–10] and Type 2M VWD[11,12] variants of A1, various complexes of WT and Type 2B variants of A1 with GPIbα,[10,13,14] function-blocking monoclonal antibodies,[8,15] DNA aptamers,[16] activating snake venoms,[9,17,18] and high-affinity directed evolution clones.[14] The structure of A1 is a αβ-Rossmann type fold with a central β-sheet flanked by six α-helices, three on each side, linked by a single disulfide bond at the N- and C-terminus. All structures of A1 are highly similar in the conformation of the backbone chain,[12] but detailed structural analyses of the complex crystal structure suggest that the rearrangement of intermolecular electrostatics between residue side chains alter the dynamics of the α1β2 loop[8,13,19] causing a pivot of the α2 helix.[20] Such a conformational propensity is supported by recent hydrogen-deuterium exchange experiments[21] and is thought to be “on—pathway” toward high—affinity.[14]

Likewise, 13 structures have been determined of WT and PT-VWD variants of free GPIbα,[22–24] GPIbα in complex with the A1 domain,[10,13,14] thrombin,[23,25,26] and a peptide

inhibitor.[27] The N-terminal domain of GPIbα that binds the A1 domain is a leucine rich repeat (LRR) domain consisting of nine parallel β strands capped by a helix containing a disulfide bond knot involving four cystines and a protruding sequence referred to as the β-switch where PT-VWD mutations reside. Several mutations causing PT-VWD have been discovered in the β-switch: W230L,[28] G233S,[29] D235Y,[30] M239I,[31] and G233V[32] and M239V,[33,34] which are the most common functionally studied variants.[35–38] In contrast to the structural similarities of A1, structures of GPIbα show that the β-switch exists as a compact partially disordered coil except when in a complex crystal structure with A1 where the β-switch exists as a β-hairpin structure of two anti-parallel β strands that continue the hydrogen bond network of the central β-sheet of the A1 domain.

Early modeling of the β-switch sequence suggested two conformers involving either a β-turn or an amphipathic helix,[39] but the observed crystal structure differences of GPIbα, free and bound to A1, immediately imply that a coil to β-hairpin transition occurs upon binding,[10] hence the name "β-switch." This structural interpretation has led to the hypothesis (Figure 1) that PT-VWD mutations shift this conformational equilibrium in favor of the β-hairpin structure.[40,41] Simulations have indicated that even fluid shear flow can induce a β-hairpin conformation[42] that is accelerated by the mutations.[43–45]

In this study, hydrogen deuterium exchange mass spectrometry (HXMS) is utilized to test this hypothesis (Figure 1) with the common GPIbα variants G233V, M239V, W230L, D235Y, and a double variant, G233V/M239V, that has found applications in clinical assays of VWF function.[46] HXMS[47] measures the steady-state time-dependent accumulation of deuterium into the protein peptide backbone. When diluted into $^{2}H_{2}O$ buffer, protein amide hydrogens exchange with solvent deuterium according to local conformational dynamics of the peptide backbone. Structurally protected amide hydrogens in stable H-bonded secondary structure (α-helix or β-sheet) exchange slowly, while amides in flexible regions of structure exchange quickly. Because the proposed structural transition involves the formation of new hydrogen bonds between amides in the antiparallel β strands, the expected HXMS observation is a reduction in the kinetics or the overall extent of deuterium incorporation into the β-switch if PT-VWD mutations shift the equilibrium towards folding. If the hydrogen exchange is enhanced by the mutations, then a partially or even intrinsically disordered coil is the thermodynamically favored conformation.

The HXMS results demonstrate that, in fact, these PT-VWD variants of GPIbα enhance hydrogen deuterium exchange in the β-switch and therefore favor a disordered conformation as the high-affinity binding competent conformation. The conclusions derived from HXMS are supported by thermodynamic unfolding measurements that show that GPIbα is destabilized by these mutations resulting in lower transition temperatures and lower unfolding enthalpies. Finally, the binding affinity is highly correlated to stability of GPIbα and the extent of hydrogen exchange within the β-switch. Cumulatively, these results, taken in the context of the recently discovered local disorder of the A1 domain in Type 2B VWD,[21,48] emphasize the role of protein chain disorder in promoting high-affinity interactions between platelets and VWF.

2 | METHODS AND MATERIALS

2.1 | Proteins

Wild-type GPIbα (amino acids H_1-E_{285} containing the signal peptide M_{-15} to Pro_0) and the mutants G233V, M239V, and the double mutant containing both mutations were expressed in the pIRES neo2 plasmid vector in HEK293 cells as a fusion construct containing an C-terminal FLAG-tag and an C-terminal Hexahistidine-tag. The A1 domain of VWF (Q_{1238}-P_{1471}) was expressed in *Escherichia coli* M15 cells as fusion proteins containing an N-terminal hexahistidine-tag using BamHI and HindIII restriction sites in the Qiagen pQE-9 plasmid.[12] All proteins were purified and their quality was confirmed by RP-HPLC and analytical gel filtration as described previously.[12,21]

Protein concentrations were measured on a Shimadzu UV2101PC spectrophotometer using the Edelhoch method as modified by Pace et al[49] from the absorption at λ = 280 nm minus twice the absorption at λ = 333 nm for the correction of light scattering. The extinction coefficients were calculated from the amino acid sequence of the complete constructs.

After purification, all proteins were dialyzed excessively into Phosphate buffered saline (PBS) or Tris buffered saline (TBS) buffer and stored for a maximum of two weeks on ice at 0°C as GPIbα aggregates upon storage at −20 or −80°C. Prior to any experiment, protein solutions were centrifuged at 60 000 *g* for at least 10 minutes to remove potential aggregation.

2.2 | Surface plasmon resonance

Surface plasmon resonance equilibrium analysis was performed on a Biacore T-100 using a CM5 (GE Healthcare) chip at 25°C. Anti-FLAG M2 antibody (Sigma-Aldrich) for capturing FLAG-tagged GPIbα was diluted into 10 mmol/L sodium acetate (pH 4.5) to 50 μg/mL concentration and immobilized covalently on active (Fc2) and reference (Fc1) channels of the CM5 chip using amine coupling kit reagents (EDC [1-ethyl-3-(3-dimethylaminopropyl) carbodiimide], NHS [N-hydroxysuccinimide] and ethanolamine). Approximately 5000 RU of anti-FLAG antibody was immobilized on both channels.

Real time interactions between vWF A1 (concentration ranging from 1 nmol/L to 8 μmol/L) and anti-FLAG captured GPIbα were measured at 25°C using HEPES buffer (pH 7.4) at a flow rate of 30 μL/min. Each binding cycle began with loading 2 μmol/L GPIbα variants for 300 seconds at a flow rate of 30 μL/min followed by 100 seconds buffer wash and injection of A1 for 100 seconds of association and 200 seconds of dissociation. Each cycle was repeated twice to verify reproducibility. In between each binding cycle, the anti-FLAG surface was regenerated with an injection of 10 mmol/L glycine at pH 2.0 for 60s. All binding responses were referenced (Fc1) and blank (buffer) subtracted before analysis to remove non-specific interactions and baseline drifts. Capture levels for GPIbα mutants were normalized to that of the wild-type GPIbα. Equilibrium responses were plotted as a function of VWF A1 concentrations and globally fitted to a solution affinity model ($RU = R_{max}c_{A1}/[K_D + c_{A1}]$), yielding the A1 dissociation constant, $K_{D,app}$, for each GPIbα variant and a shared R_{max} representing fully saturated binding.

2.3 | Differential scanning calorimetry

Differential scanning calorimetry (DSC) was performed at scan rates of 2.0, 1.5, 1.0, 0.75, 0.5, and 0.2°C/min on a TA Instruments NanoDSC at a constant pressure of 3 atm. All protein solutions (4–8 μmol/L) and the corresponding buffers were degassed under moderate stirring. The instrument was equilibrated first with several scans between 10 and 95°C with buffer loaded into the sample and reference capillaries. Then the protein was loaded into the sample capillary between two scans. The DSC trace was background corrected by subtracting the following irreversible scan as a baseline. The calculation of the excess heat capacity and the analysis using a two-state irreversible model was performed as described previously.[50,51] Equation (1) was used to fit all thermal transitions using a Microsoft Excel script (written in our laboratory) that incorporates Boole's method for numerical integration. Fitting results were minimized to the total standard deviation of the sum of squared residuals (Table S1).

2.4 | Circular dichroism and fluorescence spectroscopy

Circular dichroism (CD) measurements were performed on an Aviv Biomedical Model 420SF circular dichroism spectrometer. Fluorescence measurements were performed on a Horiba Jobin Yvon Fluorolog 3 spectrofluorometer equipped with a LFI-3751 temperature controller.

Urea-induced unfolding of WT GPIbα was monitored at 216 nm using a 1 mm quartz cell and a protein concentration of 4.8 μmol/L. Samples were incubated in their urea-containing buffer overnight at 25°C. CD signal was averaged for 10 minutes using an integration time of 1 second, corrected for the signal of the corresponding buffer and converted to mean ellipticity per amino acid residue ($[\Theta^{MRW}]$).

The kinetics of urea induced unfolding for all proteins were followed by intrinsic protein fluorescence ($\lambda_{Ex} = 280$ nm; $\lambda_{Em} = 359$ nm) at 20°C. Under rapid stirring, 2 μmol/L GPIbα was diluted 1 to 10 into buffered solutions containing a defined concentration of urea and 0.2 μmol/L protein. The following change in fluorescence signal was recorded for 10 minutes. The rates of unfolding were obtained from mono-exponential fits and averaged. Each experiment was performed as triplicate.

2.5 | Analytical size exclusion chromatography

Analytical size exclusion chromatography was performed at 25°C using an analytical Phenomenex S3000 on a Beckman Gold HPLC system. PBS buffer at a flow rate of 0.5 mL/min was used as the mobile phase and the absorption was monitored at 280 nm. Molecular mass calibration was performed using thyroglobulin (669 kDa), ferritin (440 kDa), catalase (232 kDa), aldolase (158 kDa), bovine serum albumin (67 kDa), ovalbumin (43 kDa), and soybean trypsin inhibitor (20 kDa).

2.6 | Hydrogen-deuterium exchange

Hydxogen-deuterium exchange mass spectrometry involves steady-state time-dependent HX followed by acid quenching, pepsinolysis, reverse phase separation of proteolytic fragments, and electrospray ionization orbitrap mass spectrometry.[47,52–55] HXMS was performed on

WT GPIbα and on the mutants as recently published[21] using a setup as described by Mayne et al[53] HX samples were prepared by 1–5 dilution of GPIbα into TBS in D_2O (pD 7.4). After defined times (1 minute to oven incubation at 25°C) the exchange was stopped by a drop in pD to 2.7. The quenched samples were then loaded onto a pepsin column under isocratic flow (200 μL/min) of 0.1% formic acid and proteolytic peptides were captured by a subsequent C8 trap column. After 5 minutes the trap column was switched from the isocratic flow to a water/acetonitrile gradient (20 μL/min, 1%−40% acetonitrile in 18 minutes, followed by a steep increase to 90% in 2 minutes). The gradient elutes proteolytic peptides from the C8 trap, which then become separated on a subsequent C18 column prior to injection into the LTQ Orbitrap XL for mass determination. The whole-flow system and all columns are kept in a Peltier cooled chamber at ~0°C to minimize back exchange of the incorporated deuterium during proteolysis and the separation of peptides.

Prior to the HX experiments, peptide maps containing a pool of searchable peptides for all GPIbα variants were generated using Bioworks 3.3.1 (Thermo Fisher Scientific) and the Matlab-based software EXMS 2 as previously described.[21,54] Not all of the peptides in the pool are guaranteed to be identified in any given experimental measurement. Peptide maps are given in Figure S1. Deuterated peptides were identified in EXMS2 using the generated peptide maps and an all-H experiment as reference. The subsequent HDSite analysis[55] was performed using a temperature of 25°C and a pD of 7.4 with no back exchange correction. The deuteration range was set to 0.8. After the analysis, switchable peptides were averaged manually.

3 | RESULTS

3.1 | Platelet-type VWD mutations increase the VWF A1 domain binding affinity and decrease the stability of GPIbα

The experimental parameters associated with the results of Figures 2 and 3 are given in Table S1. Binding affinity of GPIbα to the VWF A1 domain was assessed by surface plasmon resonance (SPR). Equilibrium binding curves (Figure 2A) obtained from the maximum SPR response (Figure 2B) at each concentration of the A1 domain show that the PT-VWD variants of GPIbα, G233V, M239V, G233V/M239V, and W230L increase the binding affinity. The equilibrium dissociation constant, K_D, for all PT-VWD variants is decreased relative to WT GPIbα, consistent with prior studies.[14,29,37,38,56]

The thermodynamic stability of GPIbα was assessed both by differential scanning calorimetry (Figure 3A) and urea denaturation (Figure 3B). Thermal stability of WT GPIbα and the platelet-type VWD variants of GPIbα, G233V and S, M239V and I, G233V/M239V, W230L, and D235Y, show a thermal scan rate dependency in the excess heat capacity (Figure S1) where the apparent T_M, at the peak of the transition, decreases as the scan rate is decreased. This thermodynamic behavior indicates kinetically controlled irreversible unfolding of GPIbα which is analyzed by a simple two-state irreversible model, as previously described.[50,51] Briefly, the observed excess heat capacity, $\langle C_p \rangle$, depends on the rate of unfolding, $k(T)$, equal to unity at the transition temperature, $\ln k^* = 0$ at T^*. ΔH^* is the enthalpy of the irreversible transition and ν is the thermal scan rate.

$$\langle C_p \rangle(T) = \frac{-1}{RT^2}\frac{\partial\langle H\rangle}{\partial\beta} = \frac{\Delta H^* k(T)}{\upsilon}\exp\left(\frac{1}{R\upsilon}\int\frac{k(T)}{\beta^2}d\beta\right)$$
$$\text{where } \ln\ k(T) = \ln k^* - \Delta H^*\Delta\beta$$
$$\text{and } \Delta\beta = \left(\frac{1}{RT} - \frac{1}{RT^*}\right)$$

(1)

Figure 3A shows the excess heat capacity curves at 2°C/min for each of the variants and demonstrates that all the PT-VWD variants of GPIbα unfold at lower transition temperatures and have decreased unfolding enthalpies, than WT GPIbα, indicating that the mutations significantly alter the thermodynamic stability of GPIbα.

Enthalpy is known to be proportional to the amount of polar and apolar solvent accessible surface area that becomes exposed upon thermal denaturation.[57] Given that the thermally denatured states of each of these variants are likely similar in total solvent accessibility, it is probable that the native states of the PT-VWD variants have a greater solvent accessibility than WT GPIbα. This observation is most apparent for the two variants with the M239V substitution, which have the largest change in ΔH^* relative to WT GPIbα, indicating that residue M_{239} may influence favorable interactions between the β-switch and the LRR domain that reduces the solvent accessibility of the native state of GPIbα.

Equilibrium unfolding of WT GPIbα demonstrates that the urea unfolding is also irreversible (Figure 3B), as after 72 hours of recovery from a dilution from 8 mol/L urea to 1.7 mol/L urea, GPIbα was not observed to refold to the native state circular dichroic ellipticity. The kinetic stability was therefore studied by following the kinetics of urea-induced unfolding via intrinsic protein fluorescence (Figure 3B). The kinetic traces were fit using mono-exponential functions to obtain the rate constant of the unfolding at each urea concentration. The slope of the unfolding rates was identical for all four proteins, indicating that a decreased stability but not differences in the unfolding pathway are responsible for the enhancement of the rates. Extrapolation of this linearity between the rate constants and urea concentration to 0 mol/L urea gives the rate of unfolding under native conditions. The unfolding rates of the PT-VWD variants of GPIbα were all faster than the rate for WT GPIbα, consistent with the thermal destabilization observed for these variants.

In support of the enthalpy interpretation, size exclusion chromatography shows a small decrease in the retention time (Figure 3C) of elution, which indicates, based on linear relationships between the retention time, molecular weight, and Stokes radii,[58] that the native states of the platelet-type variants have increased hydrodynamic solvation radii and, therefore, larger surface areas than the WT GPIbα.

3.2 | Platelet-type VWD mutations increase hydrogen exchange locally in the β-switch and allosterically in the leucine-rich repeats

Hydrogen-deuterium exchange mass spectrometry provides structural resolution of the mutation effects on the local dynamics of GPIbα. Figure 4A shows that the hydrogen-deuterium exchange is localized to the β-switch and the dorsum of the LRRs of GPIbα.

These exchange dynamics are mapped to the GPIbα structure in Figure 4B. Exchange in the β-switch region is altered by the mutations where HX is significantly enhanced in all the disease variants relative to WT, indicating that mutations increase the conformational flexibility of the β-switch. Concomitantly, the dorsum of the LRR exchanges significantly in the loops between the β strands and PT-VWD mutations predominantly enhance the exchange dynamics within repeats 5 and 6, particularly for W230L and D235Y. These two observations demonstrate an allosteric conformational linkage between the β-switch and the middle of the dorsum. In contrast, the LRR domain does not exchange in the palm region as a result of stable hydrogen bonds in the β-sheet.

Figure 4C shows the effect of these mutations on the deuterium incorporation of specific peptides identified in the β-switch and the LRRs of GPIbα. Relative to the unexchanged "all H" peak and the exchange of WT GPIbα at 1 hour incubation time, all of the PT-GPIbα variants have an enhanced exchange as is evident by the shift in the peptide envelopes to higher mass. This is evident in the β-switch region and allosterically in the LRR regions of LRR repeats 4, 5, and 6. Figure 4C provides the principal data in support of the site-resolved data in Figure 4A.

3.3 | Enhanced local disorder in the β-switch does not support the structure-based hypothesis

The structure-based hypothesis states that platelet-type VWD mutations should preferentially shift an equilibrium from the disordered loop conformation found in structures of GPIbα in the absence of the A1 domain to the hydrogen bonded β-hairpin structure found in complex crystal structures of GPIbα with the A1 domain present. If this were true, it is expected that HX of the β-switch would decrease as a result of stable amide hydrogen bonds formed between the β strands.

Figure 5 shows the local effects of mutations in the β-switch of GPIbα. In contrast to the expected hypothetical result, exchange is enhanced in each of the PT-VWD variants relative to WT throughout residues W_{230}-N_{242}. There are differences, however, between the local regions of the β-switch that are affected by each mutation (Figure 5A). G233V primarily enhances exchange in the N-terminal region of the β-switch between residues W_{230}-K_{237}. M239V moderately enhances exchange of residues Q_{232}-D_{235} and the C-terminal residues A_{238}-N_{242}. The double mutant, G233V/M239V, combines the effects of each of the single mutants and enhances exchange throughout the β-switch, between residues W_{230}-S_{241}, relative to WT. Exchange throughout the β-switch is also greatly enhanced by W230L and D235Y.

Mapped on the crystal structures of the β-switch in the free state (Figure 5B) and the bound state (Figure 5C), it becomes evident that the experimentally determined hydrogen exchange of the β-switch does not support a hypothesis that involves a mutation-induced shift in equilibria toward a β-hairpin structure as a binding competent conformation. To do so would involve the formation of ~6-7 additional hydrogen bonds (Figure 5C) that would effectively supress the hydrogen exchange of the β-switch. Therefore, these experiments show exactly the opposite of what is expected from the static structure perspective.

3.4 | GPIbα stability and A1 binding affinity is linked to local disorder of the β-switch

By all accounts, hydrogen-deuterium exchange and the more traditional measures of protein stability, urea and thermal denaturation, the conformational stability of GPIbα is decreased by mutations that cause platelet-type VWD. Figure 6 shows that both the stability of GPIbα and its VWF A1 domain binding affinity are correlated to the enhanced dynamics of the β-switch.

Figure 6A demonstrates that the equilibrium dissociation constant, K_D, is directly proportional to thermal transition temperature, T^*. As stability decreases, binding affinity increases. K_D is exponentially proportional to the T^* by its apparent linear relationship on the semi-logarithmic plot indicating that VWF binding is directly dependent on the stability of GPIbα over two orders of magnitude of affinity. Figure 6B demonstrates that the thermal unfolding transition temperature, T^*, and the K_D are both inversely proportional to the average exchange fraction of deuterium incorporation into residues E_{225}-V_{243} of the β-switch.

These correlations emphasize that an increase in local disorder of the β-switch decreases the global stability and increases the VWF A1 binding affinity of GPIbα. Thus, the A1 binding affinity of GPIbα is linked to the conformational dynamics of the β-switch such that the more disordered the switch becomes as a result of the mutation, the tighter the binding. An allosteric consequence of β-switch disorder is the concomitant enhanced dynamics of the LRRs (Figure 4B), which becomes particularly evident in W230L and D235Y. This allostery is supported by the loss of thermal unfolding enthalpy (Figure 3A), which indicates that the mutation also causes the β-switch to dissociate from the LRR domain of GPIbα.

4 | DISCUSSION

The present study provides a rigorous test of the hypothesis that PT-VWD mutations in GPIbα shift a conformational equilibrium away from a compact coil in favor of a hydrogen bonded antiparallel β conformation. This hypothesis (Figure 1) is presumed from crystal structures that show the β-switch as a coil in the free state[22–24] and a β-hairpin in the A1-GPIbα complex.[10,13,14] This structure-centric perspective has become so entrenched in the literature that it has become dogma,[59] but there is no published experimental evidence that such a conformational equilibrium even exists.

If the structure-based hypothesis were true, the expected experimental results of this study are two-fold. (a) PT-VWD mutations would stabilize GPIbα against unfolding. Thermal transition temperatures would increase and rates of unfolding would decrease. (b) Hydrogen exchange in the β-switch would decrease as a result of the newly formed hydrogen bonds between the antiparallel β strands resulting in a substantial decrease in the rates of exchange. Instead, GPIbα is destabilized and hydrogen exchange of the β-switch is enhanced, indicating that PT-VWD mutations increase the dynamics of local disorder in the β-switch and thereby shift the equilibrium in the opposite direction than proposed.

The presumption that the A1-GPIbα complex crystal structure is a real representation of how platelets interact with VWF has become further complexed by concepts of

blood rheology, whereby fluid shear flow is thought to promote the β-hairpin structure[42–45] outweighing any intrinsic conformational propensities to the contrary. Molecular dynamics studies have also embraced this perspective as true and compute force-dependent dissociation trajectories based on the structure of the complex to model the forces measured experimentally by single-molecule methods.[60–64] Based upon our experimental outcomes, it can be predicted that if fluid shear flow does promote the β-hairpin conformation, platelet adhesion to VWF would be inhibited, not activated. Similarly, if the single-molecule forced dissociation simulations have any bearing on reality, it is more likely that they represent dissociation from a low-affinity complex.

There are remarkably few intermolecular atomic interactions between the A1 domain and GPIbα in the complex crystal structure (Figure 1). Only five hydrogen bonds make up a direct interaction between the central β-sheet of A1 and the β-switch hairpin of GPIbα. Most of the cavity between the convex palm of GPIbα and the globular A1 domain is filled with water, which satisfies the electrostatic interactions among acidic and basic amino side chains in the interface. Contacts between the α1β2 and β2α3 loops of A1 and the N-terminal β-hairpin are more dynamic involving weak solvated electrostatic interactions with reduced electron density,[10] which tend to organize better in type 2B VWD variants of the A1 domain.[13,14] Differences between the structures of M239V and WT GPIbα in complex with A1 are reported to be minor.[13] None of the published structures have binding interfaces with optimal burial of hydrophobic residues, or favorable electrostatic complementarity between side chains and are therefore regarded as low-affinity conformations.[14]

It is possible that the β-switch is not a switch at all, as even in a complex between GPIbα and an inhibitor of VWF-platelet adhesion,[27] it exists as a coil with a small 310-helix that clamps the OS1 peptide down against the concave palm of the LLR domain. Our observations do not explicitly observe a β-hairpin conformation, but hydrogen deuterium exchange is significantly less in WT than in the PT-VWD variants (Figure 5), indicating that this sequence is more ordered in WT. Othman and Emsley[40] have suggested that a compact triangular conformation of the β-switch involving a 3_{10} helix stabilized by some hydrogen bonds and salt bridges is disrupted by PT-VWD mutations. This may explain the apparent asymmetry of the hydrogen exchange observed in the β-switch for M239V and G233V (Figure 5B). If an equilibrium between a disordered coil and more ordered structure, such as a β-hairpin or a compact triangle, is present, then the correlation between binding affinity and the extent of disorder in the β-switch predicts that the ordered conformation would result in diminished binding affinity or a loss of function. Variants with lower binding affinity, that are not associated with disease, have been reported to increase kinetic off-rates resulting in faster translocation velocities of Chinese hamster ovary cells expressing recombinant GPIb-IX complexes in flow-chamber studies.[65]

This study considers the intrinsic conformational properties of the proteins, without the complications of rheology, and demonstrates that enhanced binding affinity is proportionately determined by enhanced dynamics of the β-switch. This experimental observation supports a mechanism by which the local dynamics of the β-switch allow it to “get out of the way” so that the A1 domain can form favorable high-affinity interactions with the LRR domain of GPIbα. Such a model was proposed by Uff et al.[22] just prior to

the competing publication of the initial complex crystal structure of A1 complexed with GPIbα.[10] Considerable flexibility of the β-switch, specifically around residues G_{233} and M_{239}, is observed even in crystal structures when the structures of free GPIbα in the absence of A1 are superimposed.[14]

Viewed from a dynamics perspective, the β-switch acts like an opposable thumb[21] capable of regulating the binding of A1. The hydrogen-deuterium exchange data support a mechanism by which the β-switch exists as a coil which fluctuates between closed and open conformations (Figure 7). A lower unfolding enthalpy in the PT-VWD mutations indicates they favor an open conformation and allow A1 to bind tightly to the concave palm of the LRR domain of GPIbα. A closed conformation may induce order in the β-switch as the dynamics in WT GPIbα are significantly reduced relative to PT-VWD variants. In the closed conformation, the opposable thumb would therefore inhibit high-affinity binding by occluding accessibility to the concave surface of the LRR domain. Enhanced disorder of the opposable thumb, not only exposes this surface, but also enables a greater sampling of dynamic regions of A1 via the increased hydrophobicity caused by the mutations.[21] Similarly, extreme cases of type 2B VWD result in local disorder of the α2 helix in the A1 domain[21] allowing A1 to take advantage of conformational fluctuations in the closed state of the opposable thumb in WT GPIbα and enabling access to the LRR surface (Figure 7).

A consequence of the disorder-driven shift in probability toward an open and dynamic conformation of the β-switch is the allosteric increase in dynamics of the dorsum of the LRR domain of GPIbα. Dissociation of the β-switch allows the LRR to flex in a grasping manner. Like a hand, extension of the opposable thumb from the palm of the hand enables the hand to grasp toward a fist. Thus, the opposable thumb is naturally inhibitory to VWF binding and PT-VWD mutations remove this inhibition by shifting the probability to increasingly disordered states that concomitantly enhance the flexibility of the LRR (Figure 7).

Disorder in A1 is complementary to disorder in GPIbα and both proteins prefer binding mediated by large conformational fluctuations.[48,66] In an open conformation, GPIbα is likely to sample an ensemble of bound states with many different orientations and configurations around the A1 domain possible. Such an ensemble of bound states, partially driven by electrostatic attraction between the electronegative concave surface of the LRR and various electropositive surfaces on the A1 domain, is highly probable in PT-VWD as a result of the direct enhanced dynamics of GPIbα's opposable thumb and allosteric effects on the LRR. An ensemble of bound states could also provide clues to the loss of function Type 2M VWD since this sub-classification of VWD also involves disordered conformations caused by mutations scattered throughout the A1 domain.[48] An ensemble of possible binding configurations is also favorable to establishing erratic rheological interactions between platelets and VWF under the shear stress of blood flow where clustering of GPIbα's on platelet membranes enhances the interaction.[67]

Supplementary Material

Refer to Web version on PubMed Central for supplementary material.

ACKNOWLEDGMENTS

This work was supported by National Heart Lung and Blood Institute of the National Institutes of Health HL109109 (to M.A.) and the Great Lakes Hemophilia Foundation and Health Resources and Services Administration through the Mayo Clinic Comprehensive Hemophilia Treatment Center (M.A.). We thank Drs. Reinhard Schneppenheim and Maria Brehm for kindly providing the expression constructs for WT and PT-VWD mutants of GPIbα. We also thank Dr. Steve Whitten for the use of MPMOD in Figure 7.[68] We also gratefully acknowledge Drs. S. Walter Englander and Leland Mayne for very helpful scientific discussions regarding optimization of HXMS and the establishment of HXMS technology in our lab. In addition, we also acknowledge charitable contributions from Mark Davies' Cycle von Willebrand disease, which have defrayed, in part, publication costs.

Funding information

National Heart, Lung, and Blood Institute, Grant/Award Number: HL109109; Mayo Clinic Comprehensive Hemophilia Treatment Center; Great Lakes Hemophilia Foundation

REFERENCES

1. Fu H, Jiang Y, Yang D, Scheiinger F, Wong W, Springer T. Flow-induced elongation of von Willebrand factor precedes tension-dependent activation. Nat Commun. 2017;8(1):324. [PubMed: 28831047]
2. Othman M, Lopez J, Ware J. Platelet-type von Willebrand disease update: the disease, the molecule and the animal model. Expert Rev Hematol. 2011;4(5):475–477. [PubMed: 21939413]
3. Enayat M, Guilliatt A, Lester W, Wilde J, Williams M, Hill F. Distinguishing between type 2B and pseudo-von Willebrand disease and its clinical importance. Br J Haematol. 2006;133(6):664–666. [PubMed: 16704444]
4. Favaloro E, Patterson D, Denholm A, et al. Differential identification of a rare form of platelet-type (pseudo-) von Willebrand disease (VWD) from type 2B VWD using a simplified ristocetin-induced-platelet-agglutination mixing assay and confirmed by genetic analysis. Br J Haematol. 2007;139(4):623–626. [PubMed: 17916098]
5. Othman M, Kaur H, Favaloro E, et al. Platelet type von Willebrand disease and registry report: communication from the SSC of the ISTH. J Thromb Haemost. 2016;14(2):411–414. [PubMed: 26882161]
6. Hamilton A, Ozelo M, Leggo J, et al. Frequency of platelet type versus type 2B von Willebrand disease. An international registry-based study. Thromb Haemost. 2011;105(3):501–508. [PubMed: 21301777]
7. Emsley J, Cruz M, Handin R, Liddington R. Crystal structure of the von Willebrand factor A1 domain and implications for the binding of platelet glycoprotein Ib. J Biol Chem. 1998;273(17):10396–10401. [PubMed: 9553097]
8. Celikel R, Ruggeri Z, Varughese K. von Willebrand factor conformation and adhesive function is modulated by an internalized water molecule. Nat Struct Biol. 2000;7(10):881–884. [PubMed: 11017197]
9. Fukuda K, Doggett T, Bankston L, Cruz M, Diacovo T, Liddington R. Structural basis of von Willebrand factor activation by the snake toxin botrocetin. Structure. 2002;10(7):943–950. [PubMed: 12121649]
10. Huizinga E, Tsuji S, Romijn R, et al. Structures of glycoprotein Ibalpha and its complex with von Willebrand factor A1 domain. Science. 2002;297(5584):1176–1179. [PubMed: 12183630]
11. Tischer A, Campbell J, Machha V, et al. Mutational constraints on local unfolding inhibit the rheological adaptation of von Willebrand factor. J Biol Chem. 2016;291(8):3848–3859. [PubMed: 26677223]
12. Campbell J, Tischer A, Machha V, et al. Data on the purification and crystallization of the loss-of-function von Willebrand disease variant (p. Gly1324Ser) of the von Willebrand factor A1 domain. Data Brief. 2016;7:1700–1706. [PubMed: 27761512]
13. Dumas J, Kumar R, McDonagh T, et al. Crystal structure of the wild-type von Willebrand factor A1-glycoprotein Ibalpha complex reveals conformation differences with a complex bearing von Willebrand disease mutations. J Biol Chem. 2004;279(22):23327–23334. [PubMed: 15039442]

14. Blenner M, Dong X, Springer T. Structural basis of regulation of von Willebrand factor binding to glycoprotein Ib. J Biol Chem. 2014;289(9):5565–5579. [PubMed: 24391089]
15. Celikel R, Varughese KI, Madhusudan, Yoshioka AJW, Ware J, Ruggeri ZM. Crystal structure of the von Willebrand factor A1 domain in complex with the function blocking NMC-4 Fab. Nat Struct Biol. 1998;5(3):189–194. [PubMed: 9501911]
16. Huang R, Fremont D, Diener J, Schaub R, Sadler J. A structural explanation for the antithrombotic activity of ARC1172, a DNA aptamer that binds von Willebrand factor domain A1. Structure. 2009;17(11):1476–1484. [PubMed: 19913482]
17. Fukuda K, Doggett T, Laurenzi I, Liddington R, Diacovo T. The snake venom protein botrocetin acts as a biological brace to promote dysfunctional platelet aggregation. Nat Struct Mol Biol. 2005;12(2):152–159. [PubMed: 15665869]
18. Maita N, Nishio K, Nishimoto E, et al. Crystal structure of von Willebrand factor A1 domain complexed with snake venom, bitiscetin: insight into glycoprotein Ibalpha binding mechanism induced by snake venom proteins. J Biol Chem. 2003;278(39):37777–37781. [PubMed: 12851390]
19. Interlandi G, Yakovenko O, Tu A, et al. Specific electrostatic interactions between charged amino acid residues regulate binding of von Willebrand factor to blood platelets. J Biol Chem. 2017;292(45):18608–18617. [PubMed: 28924049]
20. Liu G, Fang Y, Wu J. A mechanism for localized dynamics-driven affinity regulation of the binding of von Willebrand factor to platelet glycoprotein Ibalpha. J Biol Chem. 2013;288(37):26658–26667. [PubMed: 23902764]
21. Tischer A, Machha V, Frontroth J, et al. Enhanced local disorder in a clinically elusive von Willebrand factor provokes high-affinity platelet clumping. J Mol Biol. 2017;429(14):2161–2177. [PubMed: 28533135]
22. Uff S, Clemetson J, Harrison T, Clemetson K, Emsley J. Crystal structure of the platelet glycoprotein Ib(alpha) n-terminal domain reveals an unmasking mechanism for receptor activation. J Biol Chem. 2002;277(38):35657–35663. [PubMed: 12087105]
23. Celikel R, McClintock R, Roberts J, et al. Modulation of alpha-thrombin function by distinct interactions with platelet glycoprotein Ibalpha. Science. 2003;301(5630):218–221. [PubMed: 12855810]
24. Varughese K, Ruggeri Z, Celikel R. Platinum-induced space-group transformation in crystals of the platelet glycoprotein Ib alpha n-terminal domain. Acta Crystallogr D Biol Crystallogr. 2004;60(Pt 3):405–411. [PubMed: 14993663]
25. Dumas J, Kumar R, Seehra J, Somers W, Mosyak L. Crystal structure of the GpIbalpha-thrombin complex essential for platelet aggregation. Science. 2003;301(5630):222–226. [PubMed: 12855811]
26. Zarpellon A, Celikel R, Roberts J, et al. Binding of alpha-thrombin to surface-anchored platelet glycoprotein Ib(alpha) sulfotyrosines through a two-site mechanism involving exosite I. Proc Natl Acad Sci USA. 2011;108(21):8628–8633. [PubMed: 21555542]
27. McEwan P, Andrews R, Emsley J. Glycoprotein Ibalpha inhibitor complex structure reveals a combined steric and allosteric mechanism of von Willebrand factor antagonism. Blood. 2009;114(23):4883–4885. [PubMed: 19726719]
28. Woods A, Sanchez-Luceros A, Bermejo E, et al. Identification of p. W246L as a novel mutation in the GP1BA gene responsible for platelet-type von Willebrand disease. Semin Thromb Hemost. 2014;40(2):151–160. [PubMed: 24474090]
29. Matsubara Y, Murata M, Sugita K, Ikeda Y. Identification of a novel point mutation in platelet glycoprotein Ibα Gly to Ser at residue 233, in a Japanese family with platelet-type von Willebrand disease. J Thromb Haemost. 2003;1(10):2198–2205. [PubMed: 14521605]
30. Enayat S, Ravanbod S, Rassoulzadegan M, et al. A novel D235Y mutation in the GP1BA gene enhances platelet interaction with von Willebrand factor in an Iranian family with platelet-type von Willebrand disease. Thromb Haemost. 2012;108(5):946–954. [PubMed: 23014764]
31. Lavenu-Bombled C, Guitton C, Dupuis A, et al. A novel platelet-type von Willebrand disease mutation (GP1BA p. Met255ILe) associated with type 2B “Malmö/New York” von Willebrand disease. Thromb Haemost. 2016;116(6):1070–1078. [PubMed: 27683759]

32. Miller JL, Cunningham D, Lyle VA, Finch CN. Mutation in the gene encoding the alpha chain of platelet glycoprotein Ib in platelet-type von Willebrand disease. Proc Natl Acad Sci USA. 1991;88(11):4761–4765. [PubMed: 2052556]
33. Russell SD, Roth GJ. Pseudo-von Willebrand disease: a mutation in the platelet glycoprotein Ib alpha gene associated with a hyperactive surface receptor. Blood. 1993;81(7):1787–1791. [PubMed: 8384898]
34. Takahashi H, Murata M, Moriki T, et al. Substitution of Val for met at residue 239 of platelet glycoprotein Ib alpha in Japanese patients with platelet-type von Willebrand disease. Blood. 1995;85(3):727–733. [PubMed: 7833477]
35. Tait AS. Phenotype changes resulting in high-affinity binding of von Willebrand factor to recombinant glycoprotein Ib-IX: analysis of the platelet-type von Willebrand disease mutations. Blood. 2001;98(6):1812–1818. [PubMed: 11535515]
36. Dong J, Schade A, Romo G, et al. Novel gain-of-function mutations of platelet glycoprotein Ibalpha by valine mutagenesis in the Cys209-Cys248 disulfide loop functional analysis under statis and dynamic conditions. J Biol Chem. 2000;275(36):27663–27670. [PubMed: 10837490]
37. Miura S, Li CQ, Cao Z, Wang H, Wardell MR, Sadler JE. Interaction of von Willebrand factor domain A1 with platelet glycoprotein Ibα-(1–289). J Biol Chem. 2000;275(11):7539–7546. [PubMed: 10713059]
38. Moriki T, Murata M, Kitaguchi T, et al. Expression and functional characterization of an abnormal platelet membrane glycoprotein Ibα (Met239Val) reported in patients with platelet-type von Willebrand disease. Blood. 1997;90(2):698–705. [PubMed: 9226170]
39. Pincus MR, Dykes DC, Carty RP, Miller JL. Conformational energy analysis of the substitution of Val for Gly 233 in a functional region of platelet GPIbα in platelet-type von Willebrand disease. Biochim Biophys Acta. 1991;1097(2):133–139. [PubMed: 1911886]
40. Othman M, Emsley J. Platelet-type von Willebrand disease: toward an improved understanding of the “sticky situation”. Semin Thromb Hemost. 2014;40(2):146–150. [PubMed: 24497122]
41. Othman M, Kaur H, Emsley J. Platelet-type von Willebrand disease: new insights into the molecular pathophysiology of a unique platelet defect. Semin Thromb Hemost. 2013;39(6):663–673. [PubMed: 23934752]
42. Han M, Xu J, Ren Y, Li J. Simulations of flow induced structural transition of the β-switch region of glycoprotein Ibα. Biophys Chem. 2016;209:9–20. [PubMed: 26656380]
43. Huang Q, Lou J, Wu J, Zhu C. Conformational transition of glycoprotein Ibα mutants in flow molecular dynamics simulation. Cell Mol Bioeng. 2011;4(3):495–504.
44. Lou J, Zhu C. Flow induces loop-to-beta-hairpin transition on the beta-switch of platelet glycoprotein Ib alpha. Proc Natl Acad Sci USA. 2008;105(37):13847–13852. [PubMed: 18772372]
45. Chen J, Tan K, Zhou H, et al. Modifying murine von Willebrand factor A1 domain for in vivo assessment of human platelet therapies. Nat Biotechnol. 2008;26(1):114–119. [PubMed: 18084279]
46. Flood V, Gill J, Morateck P, et al. Gain-of-function GPIb ELISA assay for VWF activity in the Zimmerman program for the molecular and clinical biology of VWD. Blood. 2011;117(6):e67–e74. [PubMed: 21148813]
47. Mayne L Hydrogen exchange mass spectrometry. Methods Enzymol. 2016;566:335–356. [PubMed: 26791986]
48. Tischer A, Madde P, Moon-Tasson L, Auton M. Misfolding of VWF to pathologically disordered conformations impacts the severity of von Willebrand disease. Biophys J. 2014;107(5):1185–1195. [PubMed: 25185554]
49. Pace C, Vajdos F, Fee L, Grimsley G, Gray T. How to measure and predict the molar absorption coefficient of a protein. Protein Sci. 1995;4(11):2411–2423. [PubMed: 8563639]
50. Auton M, SedlMák E, Marek J, Wu T, Zhu C, Cruz M. Changes in thermodynamic stability of von Willebrand factor differentially affect the force-dependent binding to platelet GPIBalpha. Biophys J. 2009;97(2):618–627. [PubMed: 19619477]

51. Tischer A, Cruz M, Auton M. The linker between the D3 and A1 domains of VWF suppresses A1-GPIBalpha catch bonds by site-specific binding to the A1 domain. Protein Sci. 2013;22(8):1049–1059. [PubMed: 23775931]
52. Wang L, Pan H, Smith D. Hydrogen exchange-mass spectrometry: optimization of digestion conditions. Mol Cell Proteomics. 2002;1(2):132–138. [PubMed: 12096131]
53. Mayne L, Kan Z, Chetty P, Ricciuti A, Walters B, Englander S. Many overlapping peptides for protein hydrogen exchange experiments by the fragment separation-mass spectrometry method. J Am Soc Mass Spectrom. 2011;22(11):1898–1905. [PubMed: 21952777]
54. Kan Z, Mayne L, Chetty P, Englander S. ExMS: data analysis for HX-MS experiments. J Am Soc Mass Spectrom. 2011;22(11):1906–1915. [PubMed: 21952778]
55. Kan Z, Walters B, Mayne L, Englander S. Protein hydrogen exchange at residue resolution by proteolytic fragmentation mass spectrometry analysis. Proc Natl Acad Sci USA. 2013;110(41):16438–16443. [PubMed: 24019478]
56. Kim J, Hudson N, Springer T. Force-induced on-rate switching and modulation by mutations in gain-of-function von Willebrand diseases. Proc Natl Acad Sci USA. 2015;112(15):4648–4653. [PubMed: 25810255]
57. Hilser V, Gómez J, Freire E. The enthalpy change in protein folding and binding: refinement of parameters for structure-based calculations. Proteins. 2013;26(2):123–133.
58. Uversky V Use of fast protein size-exclusion liquid chromatography to study the unfolding of proteins which denature through the molten globule. Biochemistry. 1993;32(48):13288–13298. [PubMed: 8241185]
59. Biomedicine Sadler J.. Contact–how platelets touch von Willebrand factor. Science. 2002;297(5584):1128–1129. [PubMed: 12183613]
60. Shiozaki S, Takagi S, Goto S. Prediction of molecular interaction between platelet glycoprotein Ibα and von Willebrand factor using molecular dynamics simulations. J Atheroscler Thromb. 2016;23(4):455–464. [PubMed: 26581184]
61. Ju L, Chen Y, Zhou F, Lu H, Cruz M, Zhu C. Von Willebrand factor-A1 domain binds platelet glycoprotein Ibα in multiple states with distinctive force-dependent dissociation kinetics. Thromb Res. 2015;136(3):606–612. [PubMed: 26213126]
62. Li J, Zhang L, Sun Y. Molecular basis of the initial platelet adhesion in arterial thrombosis: molecular dynamics simulations. J Mol Graph Model. 2012;37:49–58. [PubMed: 22622010]
63. Interlandi G, Thomas W. The catch bond mechanism between von Willebrand factor and platelet surface receptors investigated by molecular dynamics simulations. Proteins. 2010;78(11):2506–2522. [PubMed: 20602356]
64. Yago T, Lou J, Wu T, et al. Platelet glycoprotein Ibalpha forms catch bonds with human WT VWF but not with type 2B von Willebrand disease VWF. J Clin Invest. 2008;118(9):3195–3207. [PubMed: 18725999]
65. Kumar R, Dong J, Thaggard J, Cruz M, López J, McIntire L. Kinetics of GPIBalpha-VWFA1 tether bond under flow: effect of GPIBalpha mutations on the association and dissociation rates. Biophys J. 2003;85(6):4099–4109. [PubMed: 14645097]
66. Tischer A, Madde P, Blancas-Mejia L, Auton M. A molten globule intermediate of the von Willebrand factor A1 domain firmly tethers platelets under shear flow. Proteins. 2014;82(5):867–878. [PubMed: 24265179]
67. Gitz E, Koopman C, Giannas A, et al. Platelet interaction with von Willebrand factor is enhanced by shear-induced clustering of glycoprotein Ibα. Haematologica. 2013;98(11):1810–1818. [PubMed: 23753027]
68. Whitten S, García-Moreno B, Hilser V. Ligand effects on the protein ensemble: unifying the descriptions of ligand binding, local conformational fluctuations, and protein stability. Methods Cell Biol. 2008;84:871–891. [PubMed: 17964952]
69. Pettersen E, Goddard T, Huang C, et al. UCSF Chimera – a visualization system for exploratory research and analysis. J Comput Chem. 2004;25(13):1605–1612. [PubMed: 15264254]

Essentials

- Structures imply a disordered loop to β-hairpin transition of platelet GPIbα upon binding von Willebrand factor (VWF).
- Platelet-type von Willebrand disease mutations are hypothesized to stabilize the β-hairpin state of the A1-GPIbα complex crystal structure.
- Platelet-type von Willebrand disease variants are demonstrated to shift the conformational equilibrium in favor of a disordered loop.
- Local disorder of the β-switch establishes high-affinity binding between platelets and VWF.

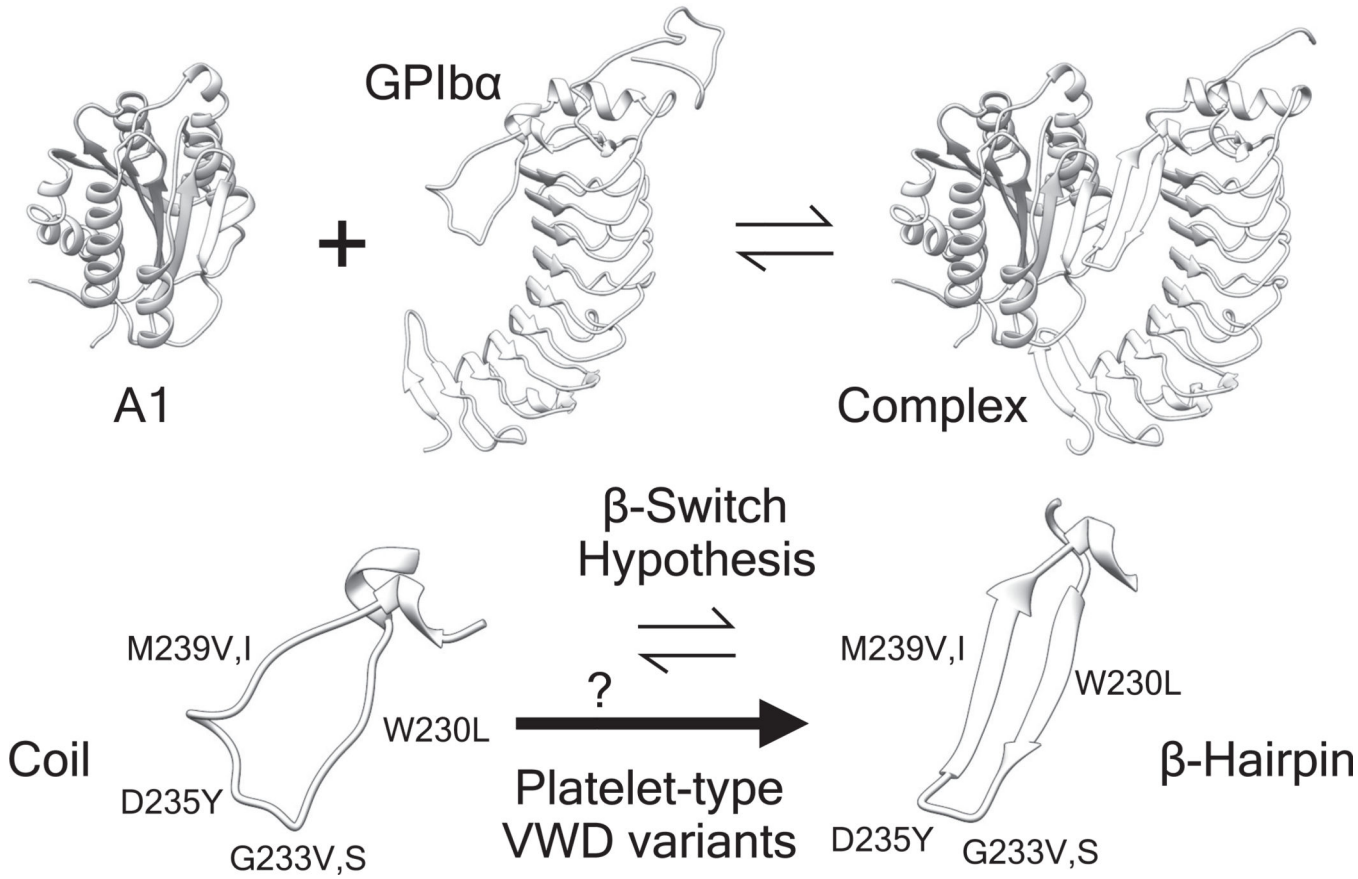

FIGURE 1.

Structure-based hypothesis. Platelet-type VWD variants in the GPIbα shift equilibrium away from the coil conformation in favor of the β-hairpin structure found in the complex crystal structure. The hypothesis is predicated on the assumption that the complex crystal structure represents the high-affinity bound state. If true, then the expectation is a stabilization of GPIbα and a decrease in hydrogen-deuterium exchange of the β-switch due to newly formed intramolecular hydrogen bonds between the β strands. A1 domain (pdb ID = 1AUQ).[7] GPIbα (pdb ID = 1GWB).[22] Complex (pdb ID = 1SQ0).[13] Rendered using UCSF Chimera.[69]

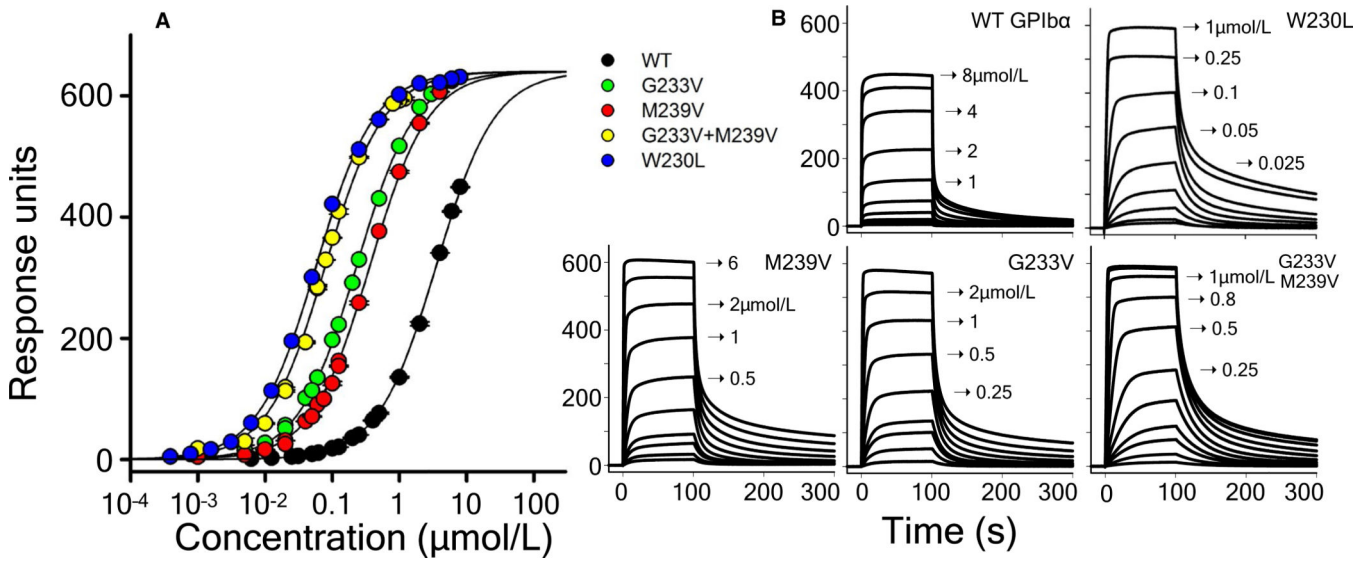

FIGURE 2.

A, Equilibrium binding of the VWF A1 domain to wild-type GPIbα and platelet-type VWD variants, W230L, G233V, M239V, G233V/G239V double mutant of GPIbα obtained from the maximum surface plasmon resonance response as a function of A1 concentration. The rank order of binding affinity is W230L > G233V/M239V > G233V > M239V > WT GPIbα. B, Representative SPR binding traces as a function of A1 concentration. See Table S1 for the dissociation constants, K_D (μmol/L)

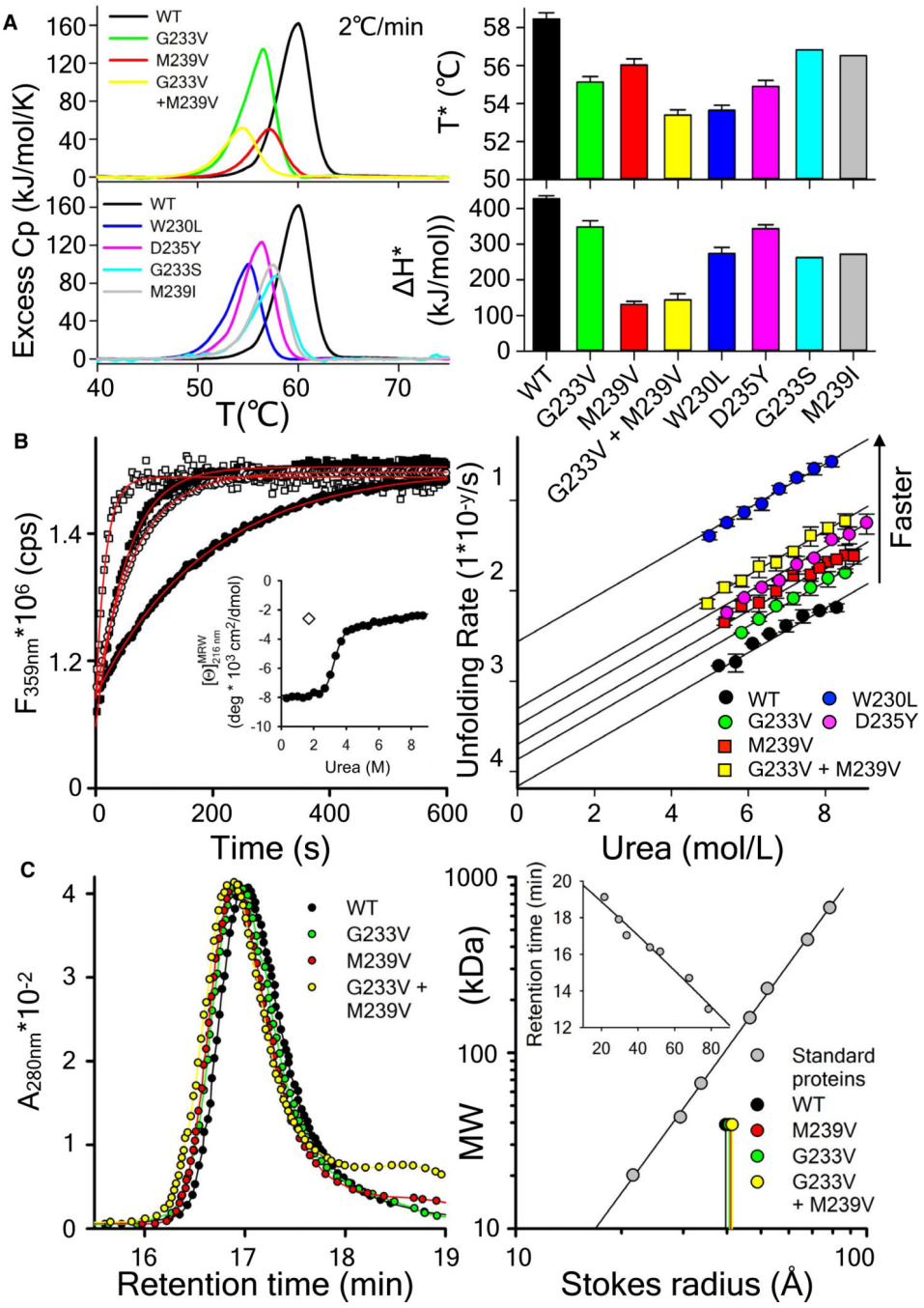

FIGURE 3.

A, Differential scanning calorimetry. Left: excess heat capacity of unfolding of wild-type GPIbα, G233V, M239V, the G233V/G239V double mutant, W230L, D235Y, G233S, and M239I at 2.0°C/min. The apparent T_M is scan rate dependent (Figure S1) and therefore kinetically irreversible. Right: For all PT-VWD variants of GPIbα, the thermal transition temperature, T^*, and the unfolding enthalpy, ΔH^*, where $k_{unf} = 1$, is less than WT GPIbα. B, Rate of urea denaturation, protein fluorescence (excitation = 280 nm, emission = 359 nm) at 20°C, is increased for all PT-VWD variants of GPIbα relative to WT GPIbα.

Left: representative kinetic traces and fits (red lines) of the urea-induced unfolding at 8.5 mol/L. Inset: urea unfolding at 25°C by circular dichroism at 216 nm is also irreversible ($c_{1/2} = 3.23 \pm 0.02$) as indicated by the diamond (dilution from 8 to 1.7 mol/L urea and incubated for 72 h). Right: unfolding rate constants of urea unfolding obtained from mono-exponential fits for each protein between 5 and 9 mol/L urea. Linear extrapolation of the rate constants to 0 mol/L urea yields rates of unfolding under native conditions in the absence of urea. C, Size exclusion chromatography. Slight shift of the elution peaks of GPIbα variants relative to WT (Left) demonstrates a non-globular conformation and variant Stokes radii (Left) that are slightly larger than WT GPIbα indicating an increased solvent accessibility. Inset: Retention time of standard proteins of known molecular weight versus their published Stokes radii.[58] Standard proteins from left to right: soybean trypsin inhibitor, ovalbumin, bovine serum albumin, aldolase, catalase, ferritin, thyroglobulin. See Table S1 for the relevant thermodynamic parameters associated with this figure

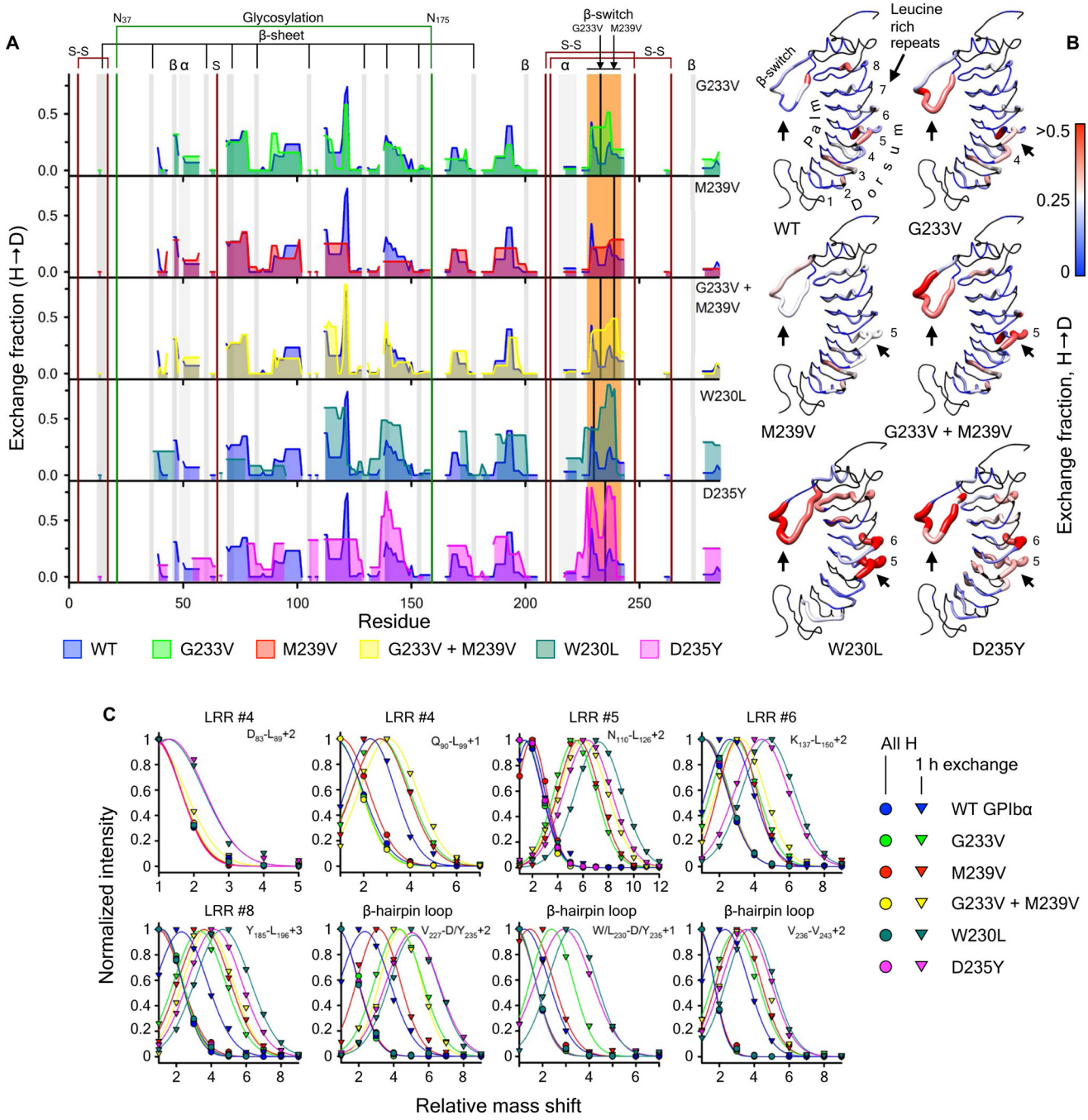

FIGURE 4.

A, Comparison of the hydrogen exchange of WT GPIbα (blue) with the platelet-type VWD variants of GPIbα from top to bottom, G233V (green, top), M239V (red), the double mutant G233V/M239V (yellow), W230L (teal), and D235Y (magenta, bottom) as a function of residue number throughout the protein at 1 h incubation time. Additional time points ranging between 60s and 24 h are presented in Figures S3–S7. HXMS was quantified in triplicate. The structural region that shows a significant difference between the variants is the β-switch (orange) loop where the mutations occur inside the disulfide knot. Allosteric

effects on dynamics are also observed in the convex LRRs 5 and 6 of the dorsum. B, Hydrogen-deuterium exchange fraction mapped onto the structure of WT GPIbα (pdb ID = 1GWB).[22] Black = not resolved, blue = 0, white = 0.25, red ≥ 0.5. Rendered using UCSF Chimera.[69] Arrows indicate the structural locations of the β-switch and the LRRs where an increased amount of hydrogen exchange in the variants is observed relative to WT GPIbα. C, Peptide envelopes (normalized intensity versus mass shift relative to the "all H" peak) of eight peptides in key regions of GPIbα. The kinetics of deuterium incorporation into specific residues in other regions of GPIbα are presented in Figures S8–S12

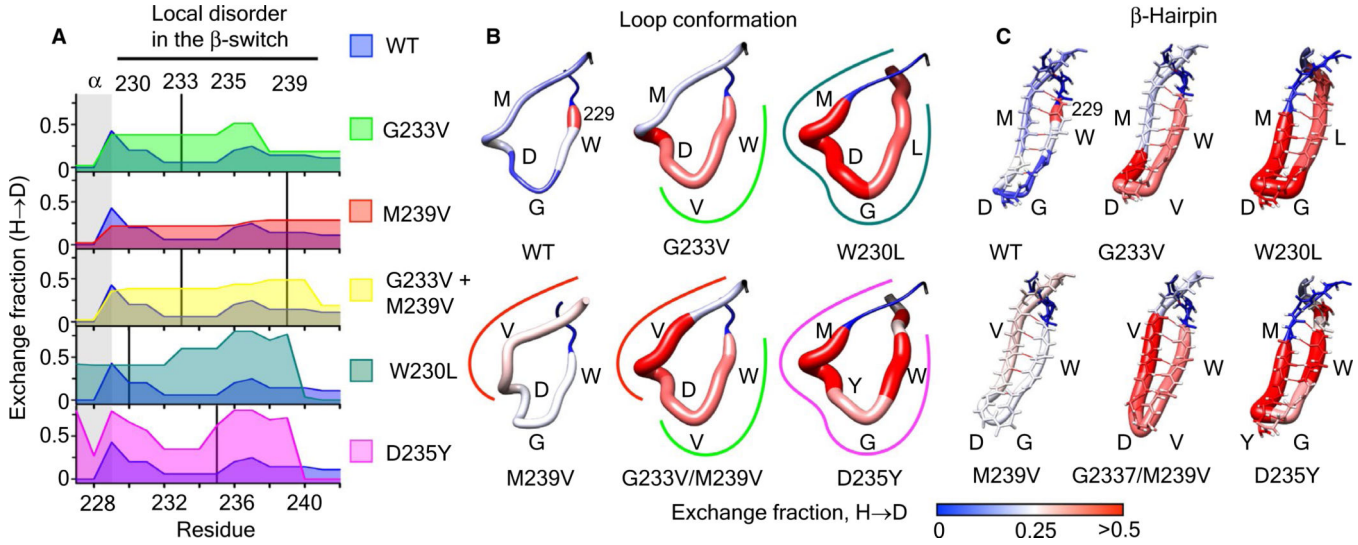

FIGURE 5.

The β-hairpin loop becomes increasingly disordered as indicated by the enhanced exchange dynamics in PT-VWD variants of GPIbα. Enhanced exchange in the loop is not supportive of the preferential formation of a β-hairpin structure in gain-of-function states. A, A zoom-in on the hydrogen-deuterium exchange fraction of residues 229–242 of the β-switch illustrating the enhanced exchange of this region in the platelet-type VWD variants compared to WT GPIbα. 1 h incubation time point. B, Hydrogen-deuterium exchange fraction mapped onto the loop structure of WT GPIbα (pdb ID = 1GWB).[22] For M239V, pdb ID = 1M0Z was used.[10] C, Hydrogen-deuterium exchange fraction mapped onto the conformation of GPIbα found in the WT complex crystal structure with A1 (pdb ID = 1SQ0).[13] For M239V, pdb ID = 1M10 was used[10] and for G233V/M239V, pdb ID = 4C2A was used.[14] Approximately 6-7 additional hydrogen bonds (red lines) are present in the structures shown in panel (C)

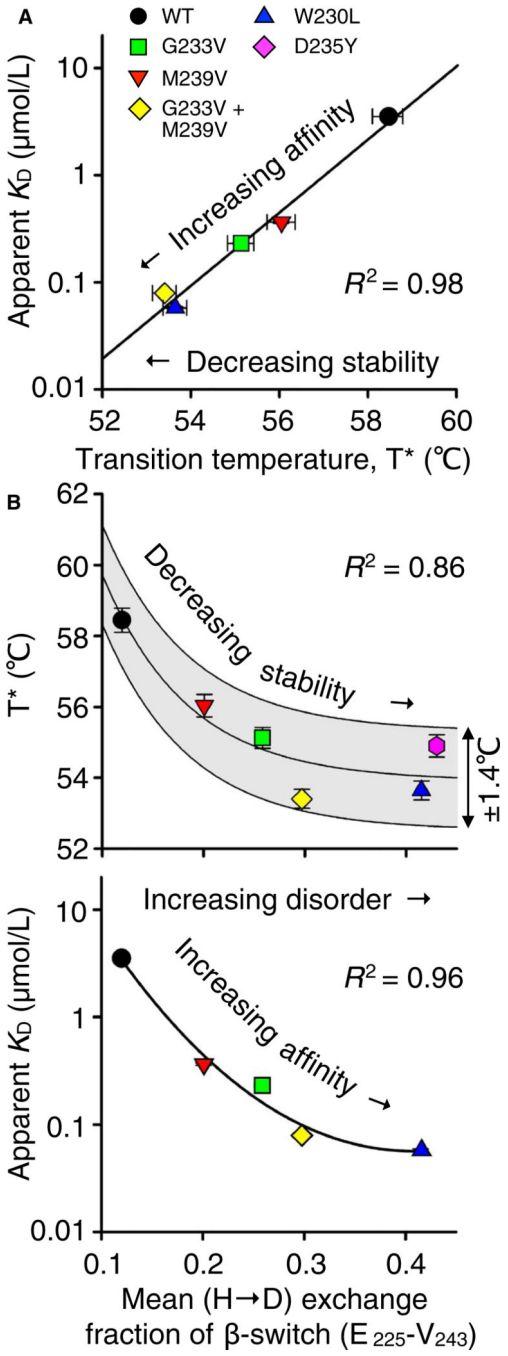

FIGURE 6.

Correlations among stability, binding affinity, and local disorder of the β-switch. A, Binding affinity, K_D, as a function of the thermal transition temperature, T^*. B, Thermal transition temperature, T^*, of GPIbα variants as a function of the average exchange fraction of the β-switch (Top). The 95% confidence interval on T^* is ~1–1.4°C. Binding affinity, K_D, as a function of the average exchange fraction of the β-switch (Bottom). β-switch residues E_{225}-V_{243} HX is at 1 h exchange incubation time. The high correlation coefficients, R^2 given

in each panel, indicate a high degree of confidence that stability and affinity are a direct consequence of the local disorder in the β-switch

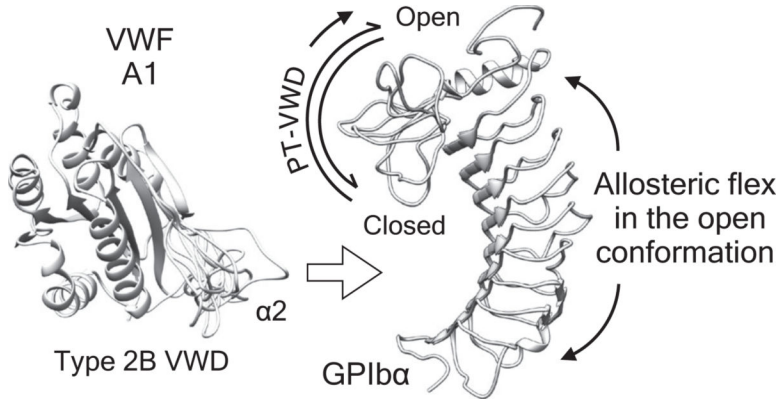

FIGURE 7.

Mechanism for disorder driven regulation of platelet GPIbα VWF A1 affinity by the β-switch of GPIbα in PT-VWD and by α2 of A1 in Type 2B VWD.[21] Models of protein chain disorder in GPIbα (pdb ID = 1GWB)[22] and A1 (pdb ID = 1AUQ),[7] generated with mini-protein modelling (MPMOD)[68] and rendered using UCSF Chimera[69]